Arsic et al., http://www.jcb.org/cgi/content/full/jcb.201102085/DC1

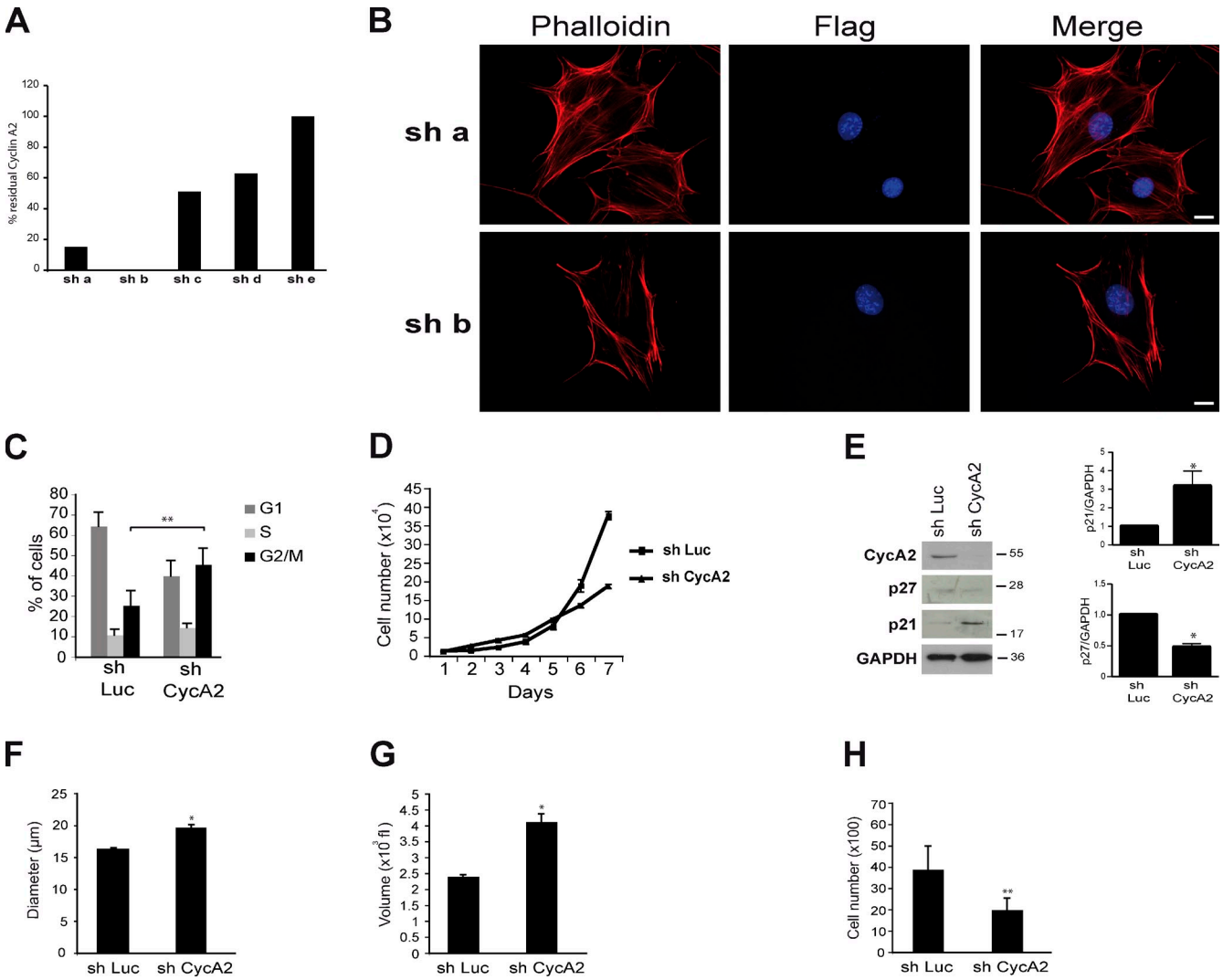

Figure S1. **Depletion of Cyclin A2 in NIH3T3 cells induces changes of several parameters.** (A) Quantification of residual Cyclin A2 protein after treatment with the different shRNAs (sh a–e) in a representative experiment. (B) Actin cytoskeleton corticalization after phalloidin staining after Cyclin A2 depletion induced by shRNA a (sh a) or shRNA b (sh b). Bars, 20 µM. (C) Cell cycle distribution of shLuc and shCycA2 NIH3T3 cells after release from a confluence block. Data are represented as means ± SEM (**, P = 0.0014; *n* = 3). (D) Growth curve of shLuc and shCycA2 NIH3T3 cells over a period of 7 d. (E, left) Western blot analysis of p21 and p27 expression in Cyclin A2–deficient cells. (right) Corresponding quantifications of three independent experiments. Molecular markers are given in kilodaltons. *, P = 0.0318. (F and G) Cell diameter (F) and cell volume (G) quantifications after Cyclin A2 depletion by shRNA (*, P = 0.05; *n* = 3). (H) Analysis of cell adherence on the plastic surface of Cyclin A2–deficient cells by comparison with shLuc-treated cells (**, P = 0.004; *n* = 3). Data are means ± SEM.

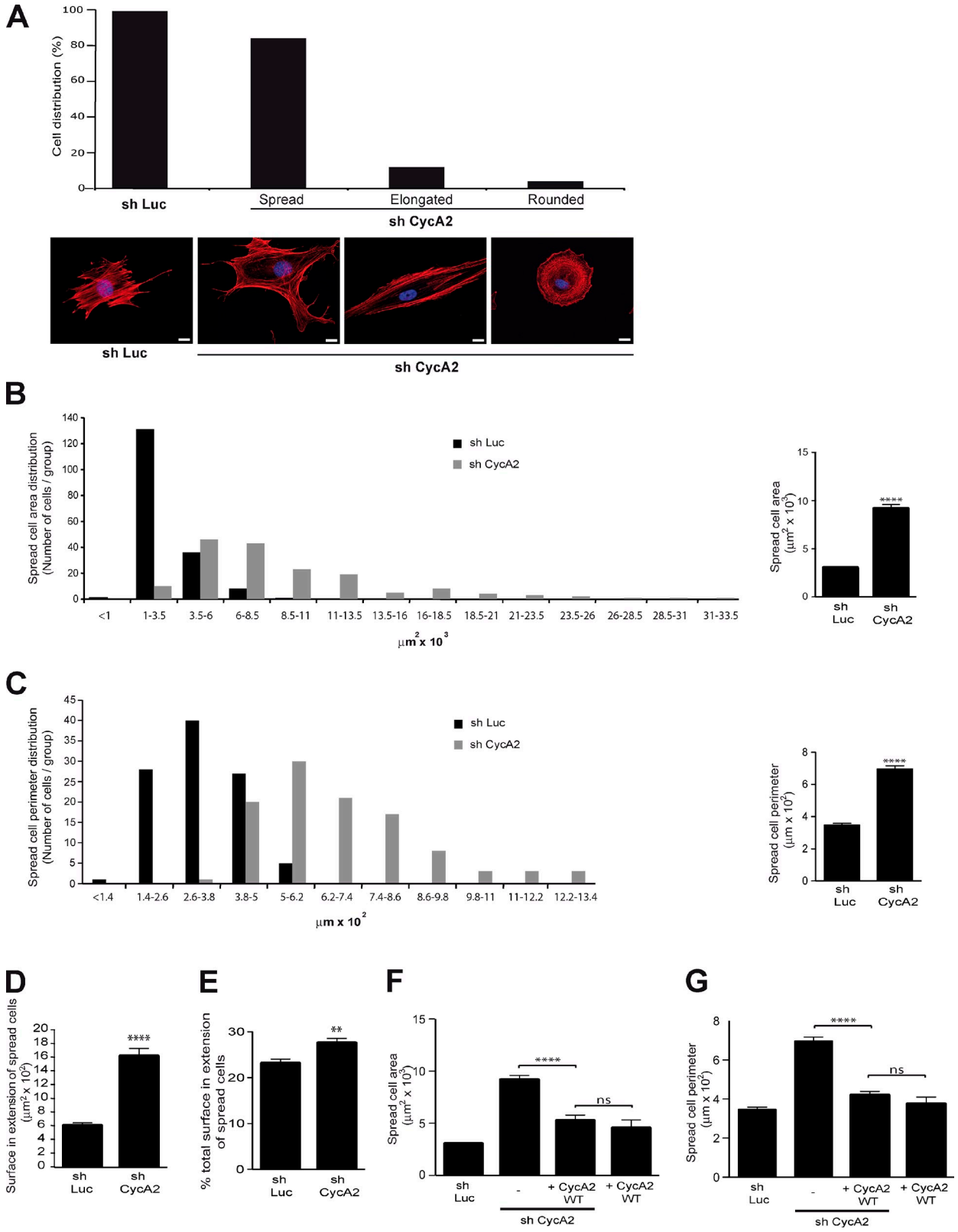

Figure S2. **Cyclin A2 depletion affects cell size and morphology.** (A) Classification of the various morphologies (spread, elongated, or rounded) of shCycA2 NIH3T3 by comparison with shLuc-treated cells of a representative experiment. Bars, 20 µM. (B and C) Quantification of spread areas (in micrometers squared; B) and perimeters (in micrometers; C) of shLuc and shCycA2 cells. (left) Cell distribution of the measured parameters. (right) Corresponding mean values represented as means ± SEM (n = 3). (D and E). Surface in micrometers squared (D) or percentage (E) of the extensions relative to that of the cell body delineated by the best circle included in the cell shape. **, P = 0.0014. (F and G) Rescue of WT cell surface (in micrometers squared; F) and cell perimeter (in micrometers; G) after Cyclin A2 expression in Cyclin A2–deficient or WT NIH3T3 cells. In this figure, all the quantifications were performed on 220–250 spread cells. Data are means ± SEM. ****, P < 0.0001.

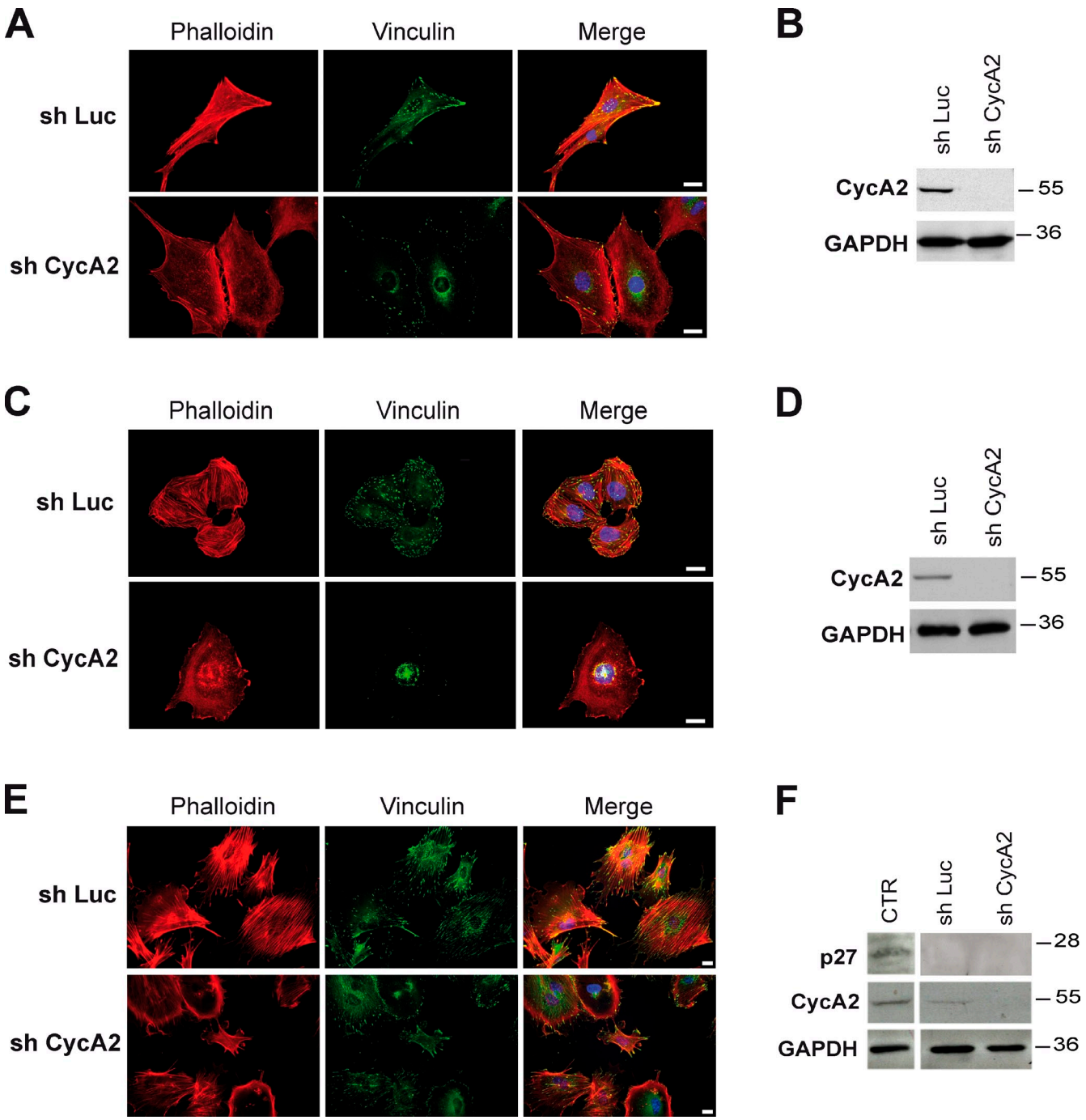

Figure S3. **Depletion of Cyclin A2 in different cell lines induces Actin cytoskeleton and adhesion plaques rearrangements as in mouse NIH3T3 cells.** (A, C, and E) Immunofluorescence analysis using phalloidin-rhodamine (red) and Vinculin (green) stainings. (A and B) Primary human skin fibroblasts. (C and D) U2OS cells. (E and F) $p27^{-/-}$ mouse embryonic fibroblasts. Bars, 20 µm. (B, D, and F) Western blot analysis of Cyclin A2 expression in shLuc and shCycA2 cells. Molecular markers are given in kilodaltons. CTR, control.

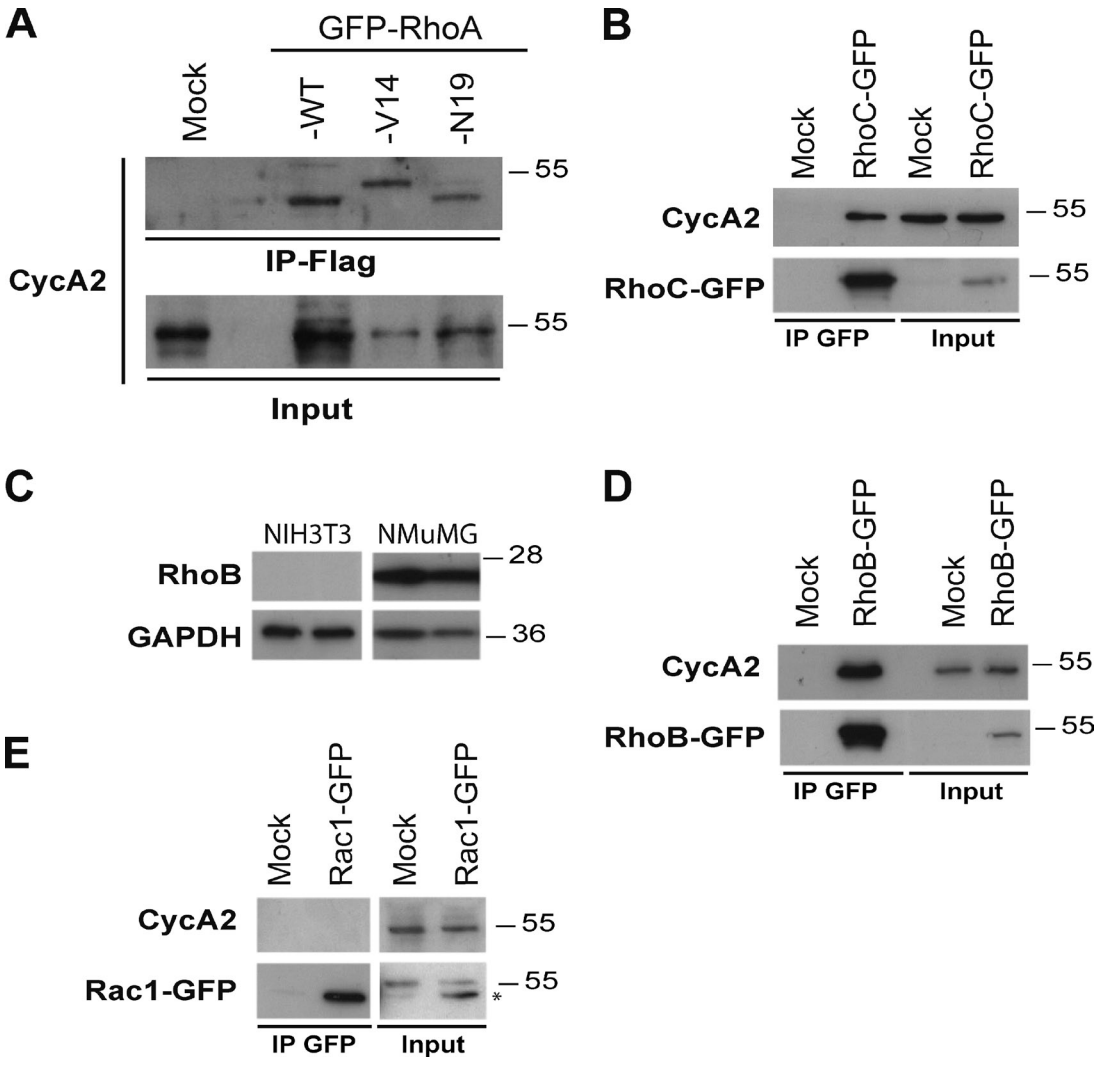

Figure S4. **Cyclin A2 interactions with Rho GTPases.** (A) Coimmunoprecipitation of endogenous Cyclin A2 with RhoA wild type (WT), dominant-negative RhoAN19, and constitutively active RhoAV14. Cell lysates obtained from NIH3T3 cells transfected with the different RhoA isoforms fused to GFP were immunoprecipitated (IP) by GFP-Trap beads. Interaction between the two molecules was detected after blotting with an anti–Cyclin A2 antibody after GFP pull-down. (B and D) Coimmunoprecipitation of endogenous Cyclin A2 with RhoC (B) and RhoB (D). NIH3T3 cell lysates overexpressing RhoC (B) or RhoB (D) were obtained after transfection of RhoC-EGFP and RhoB-EGFP, respectively. Cyclin A2 was detected using an anti–Cyclin A2 antibody after pull-down of GFP complexes. (C) Immunodetection by Western blotting of RhoB expression in NIH3T3 cells by comparison to the normal mouse mammary gland epithelial cell (NMuMG) cell line. (E) Absence of interaction between Rac1 and Cyclin A2. Complexes were precipitated from lysates derived from cells overexpressing Rac1-GFP as described in B (the asterisk marks the band corresponding to the Rac1-GFP protein). Molecular markers are given in kilodaltons.

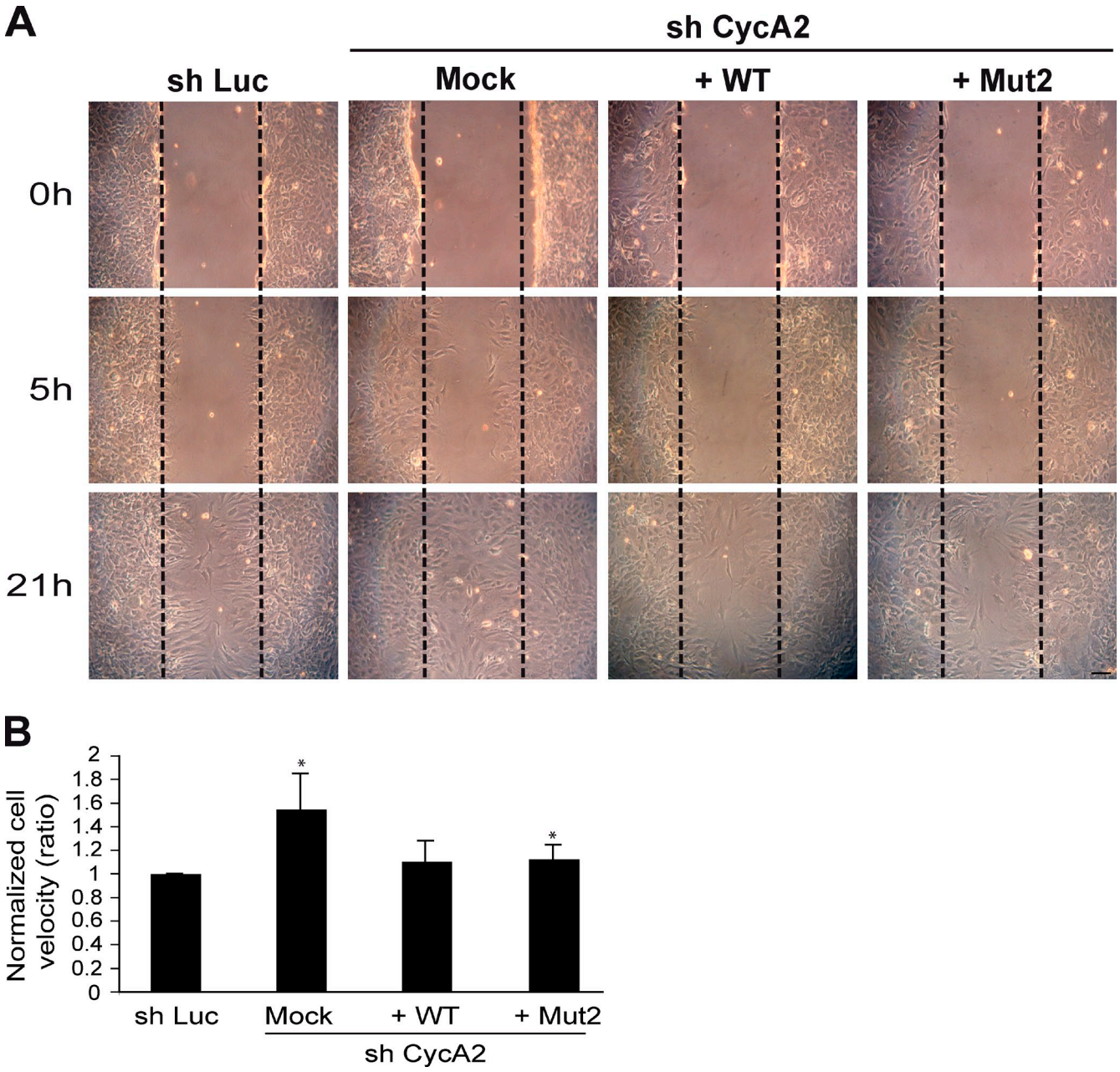

Figure S5. **Reintroduction of WT or mutant Cyclin A2 into Cyclin A2–deficient NIH3T3 cells reduces their migration ability to the level of WT cells.** (A) Wound-healing migration assay performed on confluent NIH3T3 cells infected with shLuc or shCycA2 and then transfected with an empty vector (Mock) or vectors expressing WT or Mut2-CycA2. Pictures were taken at time of scratch (t = 0), 5, and 21 h afterward. Black dotted lines indicate scratch limits. (B) Graph represents migration speeds normalized with shLuc value (*, P = 0.031 for mock infected shCycA2; *, P = 0.05 for shCycA2 cells expressing Mut2; *n* = 3). Data are means ± SEM.

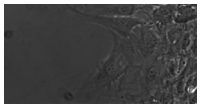

Video 1. **NIH3T3 cells were infected with shLuc retrovirus.** Cells were maintained at 37°C in humidified chamber, and their migration, in a wound-healing assay, was viewed by time-lapse microscopy using a microscope (Axiovert 200M) with a 10× Plan Neofluar 0.3 NA. Frames were taken every 5 min for 22 h. Images were collected using a camera (Micromax YHS 13001) monitored by MetaMorph software. This video corresponds to Fig. 7.

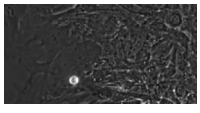

Video 2. **NIH3T3 cells were infected shCycA2 retrovirus.** Cells were maintained at 37°C in a humidified chamber, and their migration, in a wound-healing assay, was viewed by time-lapse microscopy using a microscope (Axiovert 200M) with a 10× Plan Neofluar 0.3 NA. Frames were taken every 5 min for 22 h. Images were collected using a camera (Micromax YHS 13001) monitored by MetaMorph software. This video corresponds to Fig. 7.